RESEARCH PAPER

Sintering Behavior of Lithium Meta Titanate Nanocrystallites

A. R. Abbasian[1,*], M. R. Rahimipour[2] and Z. Hamnabard[3]

* *abbasian@eng.usb.ac.ir*

Received: January 2019 **Revised:** April 2019 **Accepted:** August 2019

[1] Department of Materials Engineering, Faculty of Engineering, University of Sistan and Baluchestan, Zahedan, Iran.

[2] Ceramic Department, Materials and Energy Research Center, Karaj, Iran.

[3] Materials and Nuclear Fuel Research School, Nuclear Science and Technology Research Institute (NSTRI), Tehran, Iran.

DOI: 10.22068/ijmse.16.4.43

Abstract: *In this work, lithium meta titanate (Li_2TiO_3) nanocrystallites were synthesized by the hydrothermal method and subsequent heat treatment. The shrinkage of the powder compact was measured under constant heating rate in order to study the sintering behavior of the synthesized powders. The densification curves of the synthesized powders were also constructed via the dilatometry analysis and evaluated at several heating rates. Two separate methods, including analytical procedure and master curve sintering were employed to determine the activation energy of the initial sintering stage. Results showed that activation energy values obtained from these two distinct methods (229±14 and 230 kJ/mol, respectively) were consistent with each other. It was revealed that the dominant mechanism of densification on initial sintering of Li_2TiO_3 nanocrystallites is surface diffusion.*

Keywords: *Tritium breeding, Sintering, Activation energy, Li_2TiO_3 nanocrystallites, dilatometry.*

1. INTRODUCTION

In the development of tritium breeding ceramics, the lithium meta titanate (Li_2TiO_3) attracted considerable interests for its distinct properties as one of the most promising solid breeder materials for application in the fusion reactor blanket [1, 2]. Nanostructured Li_2TiO_3 ceramics have effective thermal conductivity, excellent tritium release behavior and good irradiation resistance [2]. The release of tritium from ceramic breeder materials involves various transport steps such as diffusion in the grain, surface reactions on the grain surface, diffusion in the pores of breeder ceramic, etc. [3]. If the mass transfer capacitance (K) is based on the diffusion in the grain, the diffusivity can be roughly evaluated using the following equation [4].

$$K = 60\frac{D}{d_p^2} \quad (1)$$

where, d_p is the diameter of the crystallite in breeder ceramic (m), and D is the tritium diffusivity in the grain (m^2/s). Therefore, the release of tritium based on the transport phenomena in the grain diffusion process could be improved due to the smaller crystallite size. Li_2TiO_3 chemical synthesis methods, such as hydrothermal [5-6] technique, usually lead to better homogenization of the particles at the molecular and atomic levels as well as nano-sized crystallite.

Sintering is an essential step in the fabrication of ceramic wares [7]. Since the various properties of the particulate body depend on this step, the consciousness of the sintering mechanism and activation energy of Li_2TiO_3 nanocrystallites becomes useful [8]. The concept of master sintering curve (MSC) initially developed by Su and Johnson [9] can be used to predict the densification behavior of a given powder and to estimate the minimum sintering activation energy [1]. This approach has been successfully applied for the sintering of micrometer-sized Li_2TiO_3 [1]. On the other hand, Matsui and co-workers [10, 11] developed a useful analytical procedure that can be used to determine the sintering mechanism at the initial sintering stage by employing the constant rate heating (CRH) technique. Although there are numerous works on sintering of ceramic powders

[DOI: 10.22068/ijmse.16.4.43]

and compacts [12, 13], to the best of our knowledge, the sintering mechanism of Li_2TiO_3 nanocrystallite powders has not been studied yet. In our previous study, CRH technique was successfully employed to study the initial sintering stage of micrometer-scale Li_2TiO_3 powder [14]. The aim of the present work is to evaluate the sintering behavior of Li_2TiO_3 nanocrystallites synthesized by hydrothermal method. Besides, the initial sintering stage of Li_2TiO_3 nanocrystallites and its corresponding activation energy was established.

2. THEORY

In MSC theory, density function Φ(ρ) is dependent on time and temperature:

$$\Phi(\rho) = \Theta(t, T(t)) \equiv \int_0^t \frac{1}{T} \exp(-\frac{Q}{RT}) dt \qquad (2)$$

where Q is the apparent activation energy of the sintering (J/mol), R is the universal gas constant, T is temperature (K), and t is time (s). In the matter above, if a unique mechanism controls the sintering process and the microstructure is only a function of density, a unique MSC can be obtained. The details of the theory have been well explained in the innovative paper by Su and Johnson [9].

Matsui et al. [10, 11] derived two sintering equations by CRH technique, as follows:

$$\ln\left[TC\frac{d\rho}{dT}\right] = \frac{-Q}{RT} + \ln[f(\rho)] + \ln\left[\frac{K\gamma\Omega D_0}{k_b}\right] - p\ln(a) \qquad (3)$$

$$\frac{d\left(\Delta L/L_0\right)}{dT} = \left(\frac{K\gamma\Omega D_0 R}{ka^p CQ}\right)^n \exp\left(\frac{nQ}{RT^{2-n}}\right).\exp\left(\frac{-nQ}{RT}\right) \qquad (4)$$

where T is temperature, C is the heating rate, $\frac{d\rho}{dT}$ is the densification rate, Q is the activation energy, R is the gas constant , $f(\rho)$ is the density function, K is the numerical constant, γ is the surface energy, Ω is the atomic volume, D_0 is the frequency factor, k_b is the Boltzmann's constant, a is the particle radius, $\Delta L, L_0 - L$ is the change in length of the compacts, L_0 is the primary length of the compacts, and the parameters n and p are the order depending on the diffusion mechanism. Equations (3) and (4) apply to the fractional shrinkages of <4%, which fulfill the initial sintering condition.

Using CRH experiments, the analysis method that can determine the diffusion mechanism at the initial sintering step is derived as follows: the activation energy is expressed using the slope of the Arrhenius-type plot of $Ln\left[TC\frac{d\rho}{dT}\right]$, S_1, against $\frac{1}{T}$ at constant density in Eq. (3):

$$Q = -RS_1 \qquad (5)$$

The apparent activation energy S_2 is expressed using the slope of the Arrhenius-type plot of $T^{2-n}\frac{d\left(\Delta L/L_0\right)}{dT}$, S_2, against $\frac{1}{T}$ In Eq. (4):

$$nQ = -RS_2 \qquad (6)$$

Since n varies between 0.31-0.53 [15], the S_2 may be estimated from the plot of $T^{1.58}\frac{d\left(\Delta L/L_0\right)}{dT}$ against $\frac{1}{T}$. By combining Eqs. (5) and (6) we have:

$$n = \frac{nQ}{Q} = \frac{S_2}{S_1} \qquad (7)$$

In this research, Eqs. (5–7) were used to determine the activation energy values and the diffusion mechanisms at the initial sintering step using the results of the CRH techniques [14].

3. EXPERIMENTAL PROCEDURE

3.1. Synthesis of Li_2TiO_3 Nanocrystallites

First, Li_2TiO_3 nanocrystallites were synthesized based on our previous work [16]. Raw materials were hydrothermally treated in 1000 mL stainless steel autoclave sealed and heated at 200 ˚C for 12 hours. The sediment materials were separated by centrifugation, washed, dried and heat-treated at 700 ˚C for 6 hours.

3.2. Sample Preparation

The synthesized Li_2TiO_3 nanocrystallites were uniaxially pressed with the loading pressure of about 300±3 MPa at room temperature to obtain a rectangular sample with dimensions of ~5×5×50

[DOI: 10.22068/ijmse.16.4.43]

mm^3. Before dilatometry testing, the compact powder was dried in an oven to eliminate any moisture. The green density determined by the geometric method was 2.0±0.04 g/cm^3. The theoretical density value was considered as 3.43 g/cm^3 [14].

3.3. Shrinkage Measurements

An optical non-contact dilatometer (Misura ODLT, Expert System, Italy) was used for monitoring the in-situ dimensional changes of the powder compact during sintering in the air atmosphere at different heating rates. The temperature was increased from room temperature to about 900 ˚C at a preset heating rate with no holding time. Then, the expansion or shrinkage changes of material in percentage were plotted versus temperature. By assuming isotropic densification of all the specimens, the relative density of the sintered sample (ρ_s) was calculated using the following equation [14].

$$\rho_s = \left[\frac{1}{1 - dL/L_0 + \alpha(T - T_0)}\right]^3 \rho_g \qquad (8)$$

where dL/L_0 is instantaneous linear shrinkage obtained by the dilatometer test, L_0 is the initial length of the specimen, T is the measured temperature, T_0 is the room temperature, ρ_g is the green density and α is the thermal expansion coefficient.

Average α value as a function of temperature was determined by equation (9) from the cooling steps of the dilatometer experiments at different heating rates adopted in our investigations. The statistical data used for the estimation of the average α value is shown in Table 1.

$$\alpha(K^{-1}) = -3.3566\times10^{-6} + 3.2034\times10^{-8}T + 1.7488\times10^{-11}T^2 \quad (25 < T < 900\,K) \qquad (9)$$

The final calculated densities after the dilatometer tests were in good agreement with those measured by the Archimedes technique.

4. RESULTS AND DISCUSSION

4.1. Characterization of the Li_2TiO_3 nanocrystallites

Fig. 1 shows the X-ray diffraction (XRD, Philips, PW 1800, Cu kα, Netherland) pattern of the synthesized Li_2TiO_3. The synthesized powder has monoclinic crystal structure.

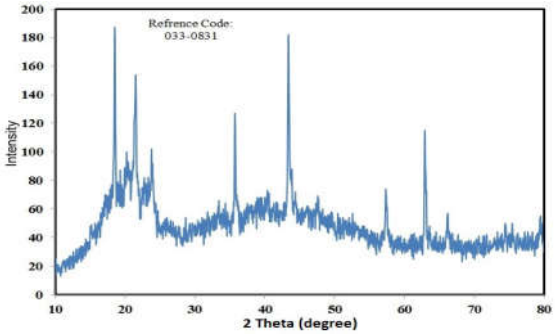

Fig. 1. XRD pattern of the Li_2TiO_3 nanocrystallite powders synthesized by hydrothermal method at 200 ˚C for 12h and subsequent heat treatment at 700 ˚C for 6h.

Scanning electron micrographs (SEM, Philips XL-30, Netherland) of the powder is shown in Fig. 2. The highly porous microstructure was due to considerable organic gas removal during heat treatment [17].

Table 1. Statistical data for calculating the thermal expansion coefficient (α) of Li_2TiO_3 nanocrystallites

Equation	$y = Intercept + B_1*T + B_2*T^2$		
Residual sum of squares	3.30252×10^{-7}		
Adj. R-square	0.94275		
Averaged Y		Value	Standard Error
	Intercept	-3.3566^{-6}	1.3686^{-6}
	B_1	3.20384^{-8}	4.44355^{-9}
	B_2	1.74884^{-11}	3.48141^{-12}

[DOI: 10.22068/ijmse.16.4.43]

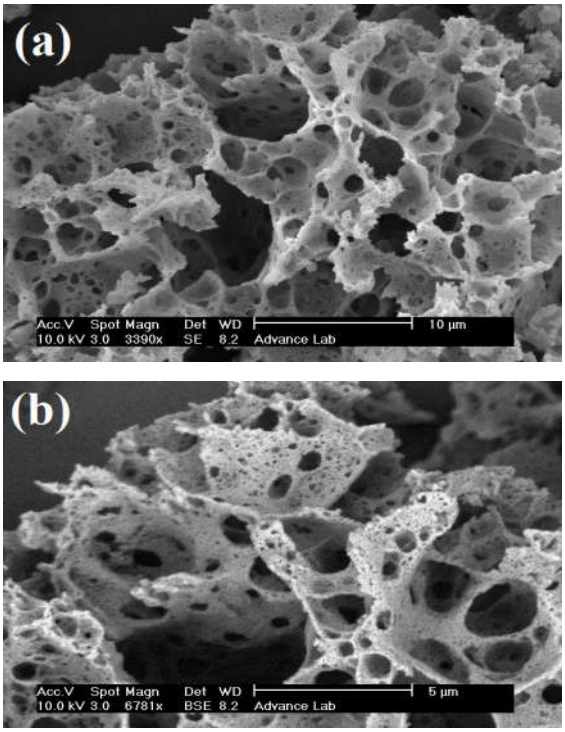

Fig. 2. (a) Secondary electron SEM micrographs of Li_2TiO_3 nanocrystallite powders synthesized by hydrothermal method at 200 ˚C for 12h and post heat-treated at 700 ˚C for 6h, (b) higher magnification micrograph of (a) at backscattered electron mode.

Transmission electron micrograph (TEM, Philips EM 208 S, Netherland) of the grounded powders is shown in Fig. 3. It is observed that the nanocrystallite powders were clusters of ultrafine particles (Fig 3a). The selected area electron diffraction (SAED) analysis is shown in Fig. 3b displaying many rings that are attributed to reflections of the monoclinic structure. The observed diffraction rings demonstrate the nanometer size of synthesized Li_2TiO_3 powder by hydrothermal route with post-heat treatment [18].

4.2. Dilatometry

Fig. 4a shows the length variations of Li_2TiO_3 nanocrystallite compact during non-isothermal sintering at three different heating rates of 2, 15 and 20 K min^{-1}. For each heating rate, the compact expanded linearly and then shrank. Apparently, increasing the heating rate shifted the onset of the initial sintering step to a higher temperature. This behavior is related to a kinetic aspect. In fact, at low heating rates, the compact is exposed for a longer time to heating and consequently experienced more shrinkage until reaching a specific temperature.

Abbasian and co-workers [14] reported that the compacted powders of commercially available Li_2TiO_3 (Aldrich Co) with the mean particle size of 23 µm heated up to 1200 ˚C didn't reach even 3.5 % shrinkage during the sintering process, while, as shown in Fig. 4a, nano-scale Li_2TiO_3 samples were significantly contracted at much lower temperatures. For example, at a heating rate of 2 K min^{-1} at about 875 ˚C, Li_2TiO_3 nanocrystallite powder synthesized by the hydrothermal method shows almost 13 % shrinkage. The higher contraction value indicates that particle size has a significant effect on the sintering behavior of Li_2TiO_3 powders. Also, Fig. 4a shows that increasing the heating rate from 15 to 20 K min^{-1} during sintering had no considerable effect on the densification behavior of Li_2TiO_3

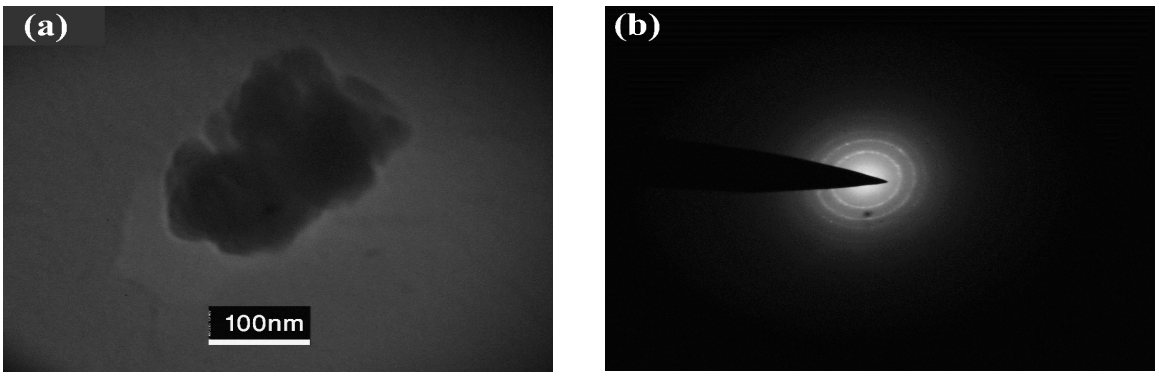

Fig. 3. (a) TEM micrographs and (b) SAED analysis of the Li_2TiO_3 nanocrystallite powders synthesized by hydrothermal method at 200 ˚C for 12h and post heat-treated at 700 ˚C for 6h.

[DOI: 10.22068/ijmse.16.4.43]

nanocrystallites and the curves are almost similar. In addition to the higher contraction of the body, the sintering temperature decreased considerably at the low heating rate of 2 K min^{-1} for the nanocrystallite powders. It is worth mentioning that the dilatometric measurements were done up to 875 ˚C, however the corresponding data in Fig. 4a are ignored due to the expansion arising from transformation of monoclinic phase to cubic phase during sintering at the heating rate of 2 K min^{-1} [19]. Additionally, end for 20 K min^{-1} is slightly less than 900 ˚C. According to Li_2O-TiO_2 phase diagram, there are two major modifications for Li_2TiO_3 including monoclinic and cubic phases. The monoclinic is a low-temperature phase that transforms into a cubic crystal structure at high temperatures [20]. Ayyub et al. [21] drafted a rule which stated that with decreasing the particle size, nanoparticles prefer the phase with higher symmetry. Since the latter phase is the high-temperature phase (the phase with the highest entropy), nanoparticles would tend to crystallize in the high-temperature phase, provided that they are small enough. Here, it is necessary to explain the term symmetry as it is used in connection with entropy. In contrast to the concept of symmetry in geometry or crystallography, where well-defined discrete points must be aligned, in statistical thermodynamics the symmetry of a system is higher; more permutations are possible, independently of the actual feasibility [22]. Therefore, the hydrothermally synthesized Li_2TiO_3 powder at the present work leads to considerably decreasing temperature for monoclinic-cubic transformation. This transformation involves expansion [19]. The monoclinic-cubic transformation occurs at about 875 ˚C, especially at low heating rate, and leads to the expansion of the body.

Jung [23] reported Li_2TiO_3 samples synthesized by the combustion synthesis method with less than 10% shrinkage at 875 ˚C which could reach 18 % at 1200 ˚C. According to Lee's report [24], Li_2TiO_3 samples fabricated by an organic-inorganic solution route showed less than 4% shrinkage at 875 ˚C and could increase to 16 % at 1200 ˚C. Wu [25] also reported that nano-size Li_2TiO_3 particles synthesized by sol-gel had less than 4% shrinkage at 875 ˚C which increases to about 13 % at 1100 ˚C. In comparison with mentioned studies, the shrinkage of the body prepared from Li_2TiO_3 powder obtained by hydrothermal method at about 875 ˚C was much higher than that of Li_2TiO_3 samples synthesized by other methods. This might be ascribed to the smaller particle size and higher activity of the powder synthesized by hydrothermal process [19]. It is worth mentioning that all the above comparisons, green bodies of the Li_2TiO_3 samples are close to each other.

Fig. 4b shows the change of shrinkage rate of Li_2TiO_3 nanocrystallite compacts during non-isothermal sintering at three different heating rates of 2, 15 and 20 K min^{-1}. It should be noted that the maximum shrinkage rate depends on the heating rate. Whatever is the temperature, the higher the heating rate, the higher is the instantaneous shrinkage rate. This tendency is also well known and has been previously reported in the case of Li_2TiO_3 materials [14]. A new phenomenon that has been observed in the sintered Li_2TiO_3 nanocrystallite body is the existence of two concave peaks instead of one concave peak in the shrinkage rate curves. The reason for this phenomenon is discussed in section 4.5.

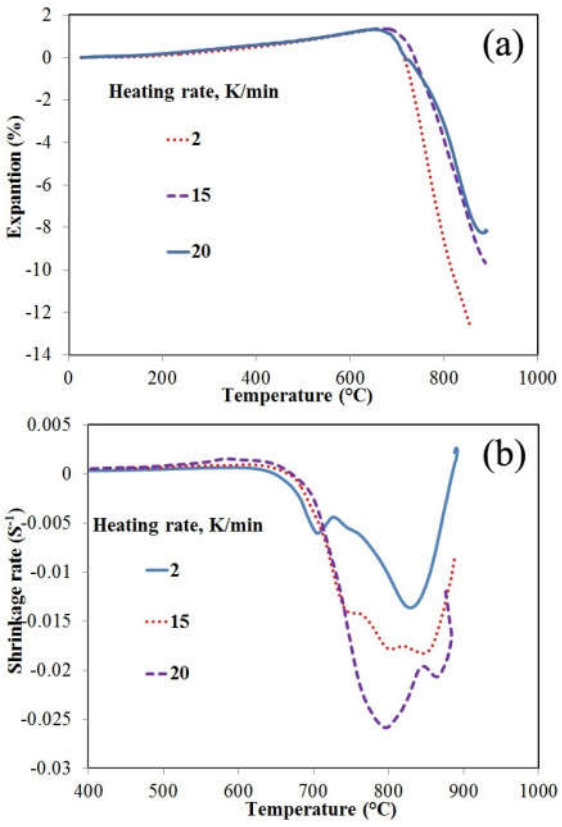

Fig. 4. Effect of heating rate (2, 15 and 20 K min^{-1}) on the contraction (a) and shrinkage rate (b) of the Li_2TiO_3 nanocrystallite compacts as a function of temperature.

[DOI: 10.22068/ijmse.16.4.43]

Based on the theoretical density of 3.43 g/cm^3 for Li_2TiO_3, the determined average green density of Li_2TiO_3 powder compacts was 2.00 g/cm^3, which is 58.31 % of theoretical density after pressing. The original shrinkage–temperature relation had been converted into the relative density-temperature relation using Eq. (8). The final calculated densities after the dilatometer experiments were in agreement with those measured by the Archimedes technique. Fig. 5 shows the dependence of density and densification rate on temperature at three different heating rates of 2, 15 and 20 K min^{-1}.

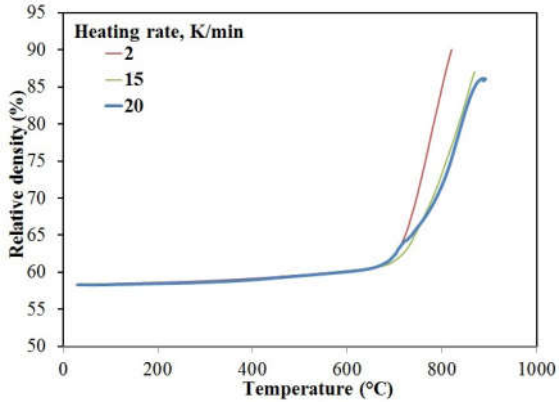

Fig. 5. The relative density of the Li_2TiO_3 nanocrystallite compacts as a function of temperature at 2, 15 and 20 K min^{-1} heating rates.

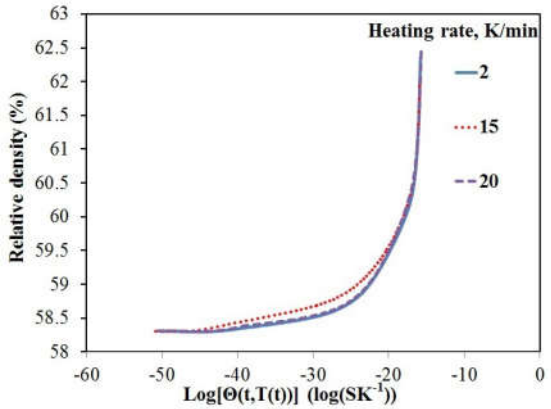

Fig. 6. The constructed MSC for sintering of Li_2TiO_3 nanocrystallite powders during initial stage (58.5%-62.5% of the theoretical density).

4.3. Construction of MSC

In this work, software developed by Pouchly and Maca [26] was used for the construction of MSC. This software calculates the MSC and finds the optimal activation energy of a given material. The MSC was calculated for Li_2TiO_3 samples using three different heating rates. A relative density range of 58.5 % – 62.5 % was used to plot the MSC. This selected range of relative density corresponds to the initial sintering stage. Fig. 6 shows the resulting MSC for the Li_2TiO_3 powder compacts. The estimated value for the sintering activation energy using the software was Q = 230 kJ/mol.

4.4. Analytical Analysis of Dilatometry Data

To examine the initial sintering stage in Li_2TiO_3 nanocrystallites, the activation energy (Q) and the apparent activation energy (nQ) of diffusion, and order on diffusion mechanism (n) can be appraised by applying Eqs. (3), (4) and (7) to the results of Fig. 4 and 5. Eq. (3) was applied in the following way. For each heating rate, both T and (dT/dt) at the same relative density the same relative density were determined and their values were plotted as $\ln[T(dT/dt)(d\rho/dT)]$ against $1/T$ (Fig. 8). In the present work, this analysis was executed in the relative density range of $58.5<\rho<62.5$ %, which corresponds to the fractional shrinkage range of <4 %. The Q at each relative density was determined from the slope of the straight line and the average value of 229±14 kJ/mol. As illustrated, each curve at certain density shows lin-

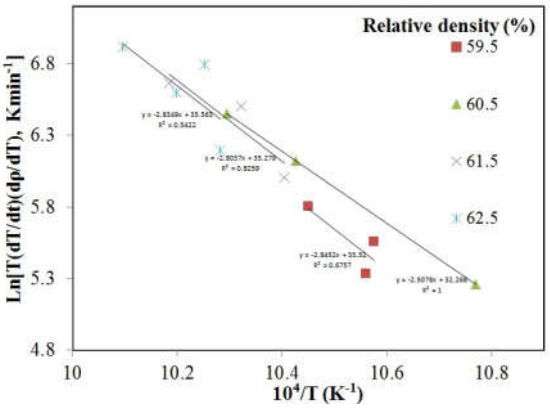

Fig. 7. Arrhenius type plots for the estimation of sintering activation energies for Li_2TiO_3 nanocrystallites according to the Matsui method.

[DOI: 10.22068/ijmse.16.4.43]

ear behavior. It should be noted that the lines are not parallel to each other in Fig. 7. This is probably due to the different mechanisms involved in sintering of Li_2TiO_3 nanocrystallites.

On the other hand, Eq. (4) was applied in the following way. In the fractional shrinkage range of <4 %, the nQ was determined from the slope of the straight line of $\ln[T^{1.6}d(\Delta L/L_0)/dT]$ plot versus $1/T$ using the shrinkage curve for each heating rate. The plots at different heating rates are shown in Fig. 8a. Contrary to the microsize Li_2TiO_3 [14], a sudden drop in the slope of curves could be observed at each heating rate, as shown in Fig. 8a. For feasible estimate of the slope of the curves in Fig. 8a, the relevant data over the low-temperature range was removed, and the linear slope of the graph was recalculated, as shown in Fig. 8b. The average value of 397±63 kJ/mol for nQ was obtained. Average values of Q and nQ were applied to equation (7) (n = 1.73).

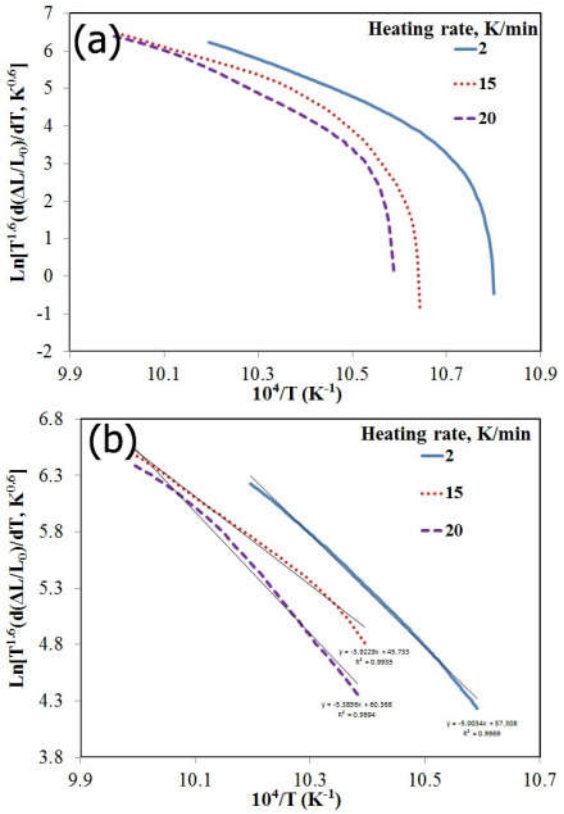

Fig. 8. (a) The plot of $\ln[T^{1.6}d(\Delta L/L_0)/dT]$ against $1/T$ for Li_2TiO_3 nanocrystallites at 2, 15 and 20 K min^{-1} heating rates, (b) Redrawn of plot (a) in which low-temperature data is removed.

According to two-sphere shrinkage models, n ranges from 0.31 to 0.33 for grain-boundary diffusion and 0.40 – 0.50 for volume diffusion from grain boundary [15]. The value of n = 1.73 is much higher than values reported for sintering mechanisms. This discrepancy may be due to surface diffusion mechanisms. Surface diffusion has low activation energy which may contribute to material transportation at or below the initial shrinkage temperature. Young and Cutler [27] have reported that surface diffusion effects can be recognized in the CRH data. As surface diffusion dominates grain boundary or volume diffusion, a sharp initial slope can be observed in the CRH data [14, 27]. As illustrated in Fig. 8a, there is an extreme curvature at shrinkage plot that may be assigned to surface diffusion, enhancing neck growth according to our previous work [14].

4.5. Microstructural Characterizations

Figure 9 shows the scanning electron micrographs (SEM, Stereo Scan 360-Leica/Cambridge, UK) of the Li_2TiO_3 nanocrystallite samples heated up to 650 °C with a heating rate of 15 K min^{-1}. As shown, a considerable porous microstructure was obtained due to the lack of contraction. The dilatometry curve at the similar heating rate (Fig. 4) did not exhibit any shrinkage up to 660 °C. On the other hand, the particles in the separate regions were agglomerated (Fig. 9a). Higher magnification images from distinct areas (Fig. 9b) show that the grains in agglomerated regions are connected firmly.

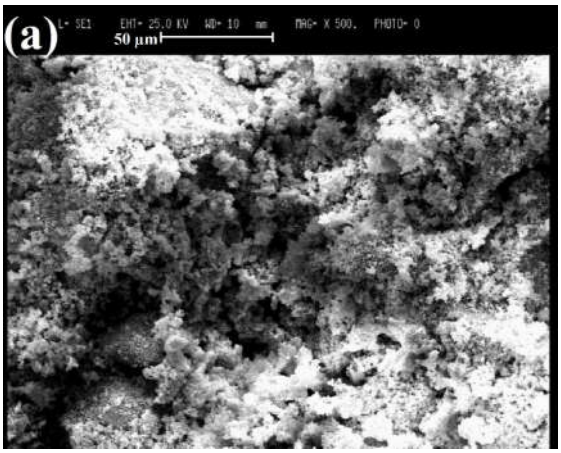

[DOI: 10.22068/ijmse.16.4.43]

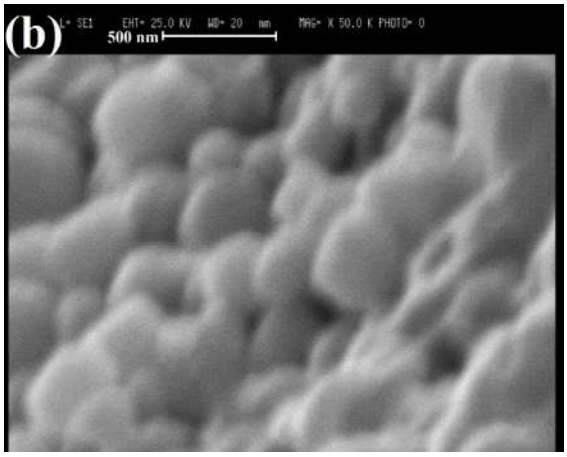

Fig. 9. SEM microstructure of Li_2TiO_3 nanocrystallites heated up to 650 ˚C at a heating rate of 15 K min^{-1} at different magnifications.

The cross-section SEM micrographs of Li_2TiO_3 nanocrystallites after the dilatometry test heated to about 875 ˚C at the heating rate of 15 K min^{-1} are shown in Fig. 10. It can be observed that the particles in the separate regions were sintered (Fig. 10a). However, a lot of porosity is yet presented between these areas. At higher magnification in Fig. 10b, there are two distinct regions in which particles are well sintered within each zone, while there is a great porosity. Fig. 10c confirms that particles were fully sintered in the form of a fine grain structure with no significant porosity. Conclusively, the fine particles in the separate agglomerated regions quickly were sintered at the lower temperatures and became utterly dense, while higher sintering temperature must be applied to the agglomerated particles. Otherwise agglomerated particles could not be densified sufficiently. Therefore, it can be claimed that the first concave peak observed in the contraction curves in Fig. 4b is related to the sintering of fine particles inside the agglomerates and the second one can be assigned to the sintering of agglomerates themselves. Therefore, according to Fig. 4b, Li_2TiO_3 nanocrystallites within the agglomerates can be sintered at temperatures as low as 706 ˚C at a heating rate of 2 K min^{-1} to obtain a fully dense agglomerate. However, the agglomerates are sintered at higher temperatures (830 ˚C), while their full densification could not be achieved. The application of Li_2TiO_3 with 80 - 85 % theoretical density was proposed in designing the blanket of a fusion reactor [28]. So, the hydrothermally synthesized Li_2TiO_3 powders at this work have a high potential for successful application in fusion reactor.

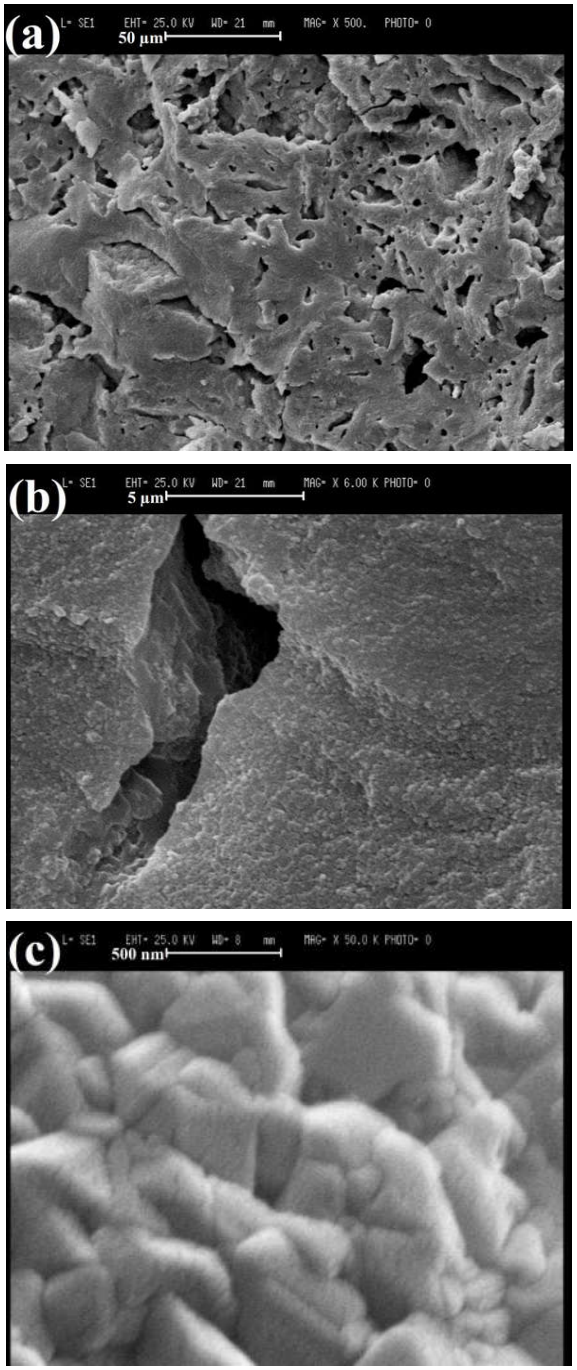

Fig. 10. Cross section microstructure of Li_2TiO_3 nanocrystallites heated up to 875 ˚C at a heating rate of 15 K min^{-1} at different magnifications.

[DOI: 10.22068/ijmse.16.4.43]

5. CONCLUSIONS

The conclusions of this research can be summarized as follows:

- During the initial sintering stage, the activation energy value of Li_2TiO_3 nanocrystallites determined using MSC approach was 230 kJ/mol, which was in good agreement with that calculated values by Matsui et al. method (Q = 229±14 kJ/mol).
- The dominant sintering mechanism of Li_2TiO_3 nanocrystallites at the initial sintering stage was surface diffusion.
- Two concave peaks instead of one concave peak were observed in the shrinkage rate curves during the sintering of Li_2TiO_3 nanocrystallites. The first concave peak was related to the sintering of fine particles inside the agglomerates and the second one was assigned to the sintering of agglomerates themselves.

ACKNOWLEDGMENT

This work was supported by Nuclear Science and Technology Research Institute. Also, the authors acknowledge Mahdi Shafiee Afarani and Mahmoud Sharifitabar for editing the manuscript.

REFERENCES

1. Abbasian, A. R., M. R. Rahimipour, and Z. Hamnabard. "Activation Energies for Initial and Intermediate Stage Sintering of Li_2TiO_3 Determined by a Two-Stage Master Sintering Curve Approach". in Advances in Engineering Mechanics and Materials 2014, Santorini Island, Greece.
2. Wang, H., M. Yang, Y. Gong, L. Feng, C. Dang, Y. Shi, Q. Shi, J. Wei, Z. Liao, and T. Lu, "Fabrication of nanostructured Li_2TiO_3 ceramic pebbles as tritium breeders using powder particles synthesised via a CTAB-assisted method. Ceram". Int., 2017, 43, 5680-5686.
3. Casadio, S., J. G. van der Laan, C. Alvani, A. J. Magielsen, and M. P. Stijkel, "Tritium release kinetics from Li_2TiO_3 pebbles as prepared by soft-wet-chemistry". J. Nucl. Mater., 2004, 329–333, Part B, 1252-1255.
4. Munakata, K., A. Koga, Y. Yokoyama, S. Kanjo, S. Beloglazov, D. Ianovski, T. Takeishi, R. D. Penzhorn, K. Kawamoto, H. Moriyama, Y. Morimoto, S. Akahori, and K. Okuno, "Effect of water vapor on tritium release from ceramic breeder material". Fusion Eng. Des., 2003, 69, 27-31.
5. Khaksar, E., M. Shafiee Afarani, and A. Samimi, "In Situ Solvothermal Crystallization of TiO_2 Nanostructure on Alumina Granules for Photocatalytic Wastewater Treatment". J. Mater. Eng. Perform., 2014, 23, 92-100.
6. Yu, C. L., K. Yanagisawa, S. Kamiya, T. Kozawa, and T. Ueda, "Monoclinic Li_2TiO_3 nano-particles via hydrothermal reaction: Processing and structure". Ceram. Int., 2014, 40, 1901-1908.
7. T. Ebadzadeh , S. G., Mas. Alizadeh , K. Asadian , Y. Ganjkhanlou, "The Effects of ZnO Additive on Sintering Behavior, Microstructural Evolution and Microwave Dielectric Properties of Li_2TiO_3 Ceramics. Iran. J. Mater. Sci. Eng., 2019, 16.
8. Pouchly, V., J. Hruby, and K. Maca, "A Practical Approach for the Calculation of the Activation Energy of the Sintering". Sci. Sinter., 2017, 48, 317-324.
9. Su, H. and D. L. Johnson, "Master Sintering Curve: A Practical Approach to Sintering". J. Am. Ceram. Soc., 1996, 79, 3211-3217.
10. Matsui, K., N. Ohmichi, M. Ohgai, N. Enomoto, and J. Hojo, "Sintering Kinetics at Constant Rates of Heating: Effect of Al_2O_3 on the Initial Sintering Stage of Fine Zirconia Powder". J. Am. Ceram. Soc., 2005, 88, 3346-3352.
11. Matsui, K., K. Tanaka, N. Enomoto, and J. Hojo, "Sintering kinetics at constant rates of heating: effect of alumina on the initial sintering stage of yttria-stabilized cubic zirconia powder". J. Ceram. Soc. Jpn., 2006, 114, 763-768.
12. Falamaki, C., M. S. Afarani, and A. Aghaie, "Initial sintering stage pore growth mechanism applied to the manufacture of ceramic membrane supports". J. Eur. Ceram. Soc., 2004, 24, 2285-2292.
13. Shafiee Afarani, M., A. Samimi, and E. Bahadori Yekta, "Synthesis of alumina granules by high shear mixer granulator: Processing and sintering". Powder Technol., 2013, 237, 32-40.
14. Abbasian, A. R., M. R. Rahimipour, and Z. Hamnabard, "Initial Sintering Kinetics of Lithium Meta Titanate at Constant Rates of Heating". Iran. J. Mater. Sci. Eng., 2013, 10, 44-53.

[DOI: 10.22068/ijmse.16.4.43]

15. Johnson, D. L., "New Method of Obtaining Volume, Grain-Boundary, and Surface Diffusion Coefficients from Sintering Data". J. Appl. Phys., 1969, 40, 192-200.
16. Abbasian, A. R., M. R. Rahimipour, and Z. Hamnabard, "Hydrothermal Synthesis of Lithium Meta Titanate Nanocrystallites". Procedia Mater. Sci., 2015, 11, 336-341.
17. Shahmirzaee, M., M. Shafiee Afarani, A. M. Arabi, and A. Iran Nejhad, "In situ crystallization of $ZnAl_2O_4$/ZnO nanocomposite on alumina granule for photocatalytic purification of wastewater". Res. Chem. Intermed., 2017, 43, 321-340.
18. Mostaan, H., M. Z. Mehrizi, M. Rafiei, R. Beygi, and A. R. Abbasian, "Contribution of mechanical activation and annealing in the formation of nanopowders of Al(Cu)/TiC-Al_2O_3 hybrid nanocomposite". Ceram. Int., 2017, 43, 2680-2685.
19. Abbasian, A. R., Rahimipour, M. R. and Hamnabard, Z., "Phase transformation during sintering of Li_2TiO_3 nanocrystallites synthesised by hydrothermal method". Micro Nano Lett., 2016, 11, 822-824.
20. Kleykamp, H., "Phase equilibria in the Li–Ti–O system and physical properties of Li_2TiO_3". Fusion Eng. Des., 2002, 61, 361-366.
21. Ayyub, P., V. Palkar, S., "Chattopadhyay, and M. Multani, Effect of crystal size reduction on lattice symmetry and cooperative properties". Phys. Rev. B, 1995, 51, 6135.
22. Vollath, D., "Nanomaterials: An Introduction to Synthesis, Properties and Applications", ed. S. Edition. 2013, Wiley-Vch.
23. Jung, C. H., "Sintering characterization of Li_2TiO_3 ceramic breeder powders prepared by the solution combustion synthesis process". J. Nucl. Mater., 2005, 341, 148-152.
24. Lee, S. J., "Characteristics of lithium titanate fabricated by an organic-inorganic solution route". J. Ceram. Process. Res., 2008, 9, 64-67.
25. Wu, X., Z. Wen, B. Lin, and X. Xu, "Sol–gel synthesis and sintering of nano-size Li_2TiO_3 powder". Mater. Lett., 2008, 62, 837-839.
26. Pouchly, V. and K. Maca, "Master Sintering Curve – A Practical Approach to its Construction Sci. Sinter", 2010, 42, 25-32.
27. Young, W. S. and Cutler, I. B., "Initial Sintering with Constant Rates of Heating". J. Am. Ceram. Soc., 1970, 53, 659-663.
28. Tsuchiya, K., H. Kawamura, M. Uchida, S. Casadio, C. Alvani, and Y. Ito, "Improvement of sintered density of Li_2TiO_3 pebbles fabricated by direct-wet process". Fusion Eng. Des., 2003, 69, 449-453.

[DOI: 10.22068/ijmse.16.4.43]